ELSEVIER

Journal of Alloys and Compounds 275–277 (1998) 295–300

Journal of ALLOYS AND COMPOUNDS

Absorption and fluorescence spectra of Am^{3+}-doped $Cs_2NaLuCl_6$ elpasolite crystals

Yu.A. Barbanel'*, G.P. Chudnovskaya, R.B. Dushin, V.V. Kolin, V.P. Kotlin, S.N. Nekhoroshkov, M.V. Pen'kin

V.G. Khlopin Radium Institute, 2nd Murinskii Ave. 28, St. Petersburg 194021, Russia

Abstract

Low-temperature absorption and fluorescence (including self-fluorescence) spectra of Am^{3+} in the elpasolite lattice have been studied in the regions of the $^7F_6 \leftarrow {}^7F_0$ and $^5L_6 \rightarrow {}^7F_0$ transitions, correspondingly. Ten crystal field sublevels in the $^7F_6$ and $^5L_6$ levels have been localized and assigned. The crystal field parameters have been calculated for the $AmCl_6^{3-}$ complex. © 1998 Elsevier Science S.A.

Keywords: Americium; Elpasolites; Absorption spectra; Fluorescence spectra; Crystal field

1. Introduction

Optical spectroscopic studies of the Ln^{3+}-doped elpasolites, where the 4f ions are situated at the sites of an ideal O_h symmetry, have been rather extensive in the two recent decades [1]. The Am^{3+} ($5f^6$) ion has been the first trivalent actinide for which analogous researches were undertaken. Absorption spectra of Am^{3+} in the chloroelpasolite lattice were first obtained (as the spectra of *neat* $Cs_2NaAmCl_6$ [2]) soon after the first syntheses of this compound by evaporation of an aqueous solution [3] and by crystallization of a stoichiometric melt [4] (methods E and A, correspondingly, in notation of Ref. [4]). The spectra in Ref. [2] were recorded for both molten (1023 K) and solid (298–973 K) $Cs_2NaAmCl_6$. At lower temperatures, vibronic patterns were observed in selected spectral regions, which showed the O_h symmetry of the Am^{3+} surrounding. However, no vibronic and sublevel assignments were made in that work, mainly because of the poor resolution in the vibronic features. The well-resolved absorption spectra were obtained at 298 and 77 K for $Cs_2NaLuCl_6$:Am^{3+} in the regions of the ($^5G_2$, $^5D_2$, $^7F_2$)$\leftarrow {}^7F_0$ [5], which enabled us to assign the vibronic lines basing on a factor-group analysis of the vibrational modes for the elpasolite structure. As a result, the Γ_3 and Γ_5 crystal field (CF) sublevels were localized for the $J=2$ excited states at energies corresponding to the strictly forbidden in O_h symmetry zero-phonon (0–0) transitions. For the same crystal, we obtained the absorption spectra of Am^{3+} in the regions of the $^7F_4 \leftarrow {}^7F_0$ and $^7F_6 \leftarrow {}^7F_0$ transitions at 298 and 77 K [6]. However, being unable at that time to take helium temperature spectra at the Khlopin Institute, we could not assign fairly complex vibronic features associated with the $J=4$ and $J=6$ excited levels. The vibronic and CF assignments for the $^7F_4 \leftarrow {}^7F_0$ transition were presented in Ref. [7]. One of the aims of this work was to assign the vibronic lines in the low-temperature absorption spectra of Am^{3+} in the region of the $^7F_6 \leftarrow {}^7F_0$ transition and to localize the forbidden zero-phonon transitions to the sublevels of the excited $^7F_6$ state.

The first luminescence spectra of Am^{3+} were obtained in studies of the ^{243}Am-doped $Cs_2NaLaCl_6$ crystal [8,9]. Both self-luminescence (due to α-decay energy) and laser-excited luminescence spectra of Am^{3+} were recorded at 298 and 77 K, which enabled the first detection of the $^5D_1$ excited state in the $5f^6$ configuration (16 850 cm^{-1}) for a crystalline matrix. Also, the splitting of the $^7F_2$ level (410 cm^{-1} at 77 K), determined previously from the $^7F_2 \leftarrow {}^7F_0$ transition in the infrared absorption spectrum [5], was confirmed [8,9] by studying the $^5D_1 \rightarrow {}^7F_2$ luminescent transition. The self-luminescence spectra of the $^{241}Am^{3+}$-doped $Cs_2NaLuCl_6$ crystal, taken at 298 and 77 K [10], proved much more intense and well-resolved (especially in the region of the $^5L_6 \rightarrow {}^7F_0$ transition) compared to those for ^{243}Am. Nevertheless, no vibronic and CF assignments were made [10]. Study of the temperature dependence of the Am^{3+} luminescence spectra down to 15 K, and

*Corresponding author. Fax: +7 812 2475781; e-mail: barbanel@rad.spb.su

0925-8388/98/$19.00
PII: S0925-8388(98)00321-1

assignment of both the vibronic and CF states in the region of the $^5L_6 \rightarrow {}^7F_0$ transition, was another aim of this work.

2. Experimental

The $Cs_2NaLuCl_6:Am^{3+}$ crystals were prepared by melting stoichiometric amounts of CsCl, NaCl and MCl_3 (M= Lu, Am) in an HCl flow (method A in Ref. [4]) with subsequent crystal growth by the Bridgeman method.

The absorption spectra of the $Cs_2NaLuCl_6$ crystal, doped with 5 mol.% ^{243}Am (half-life, 7368 years), were measured on an SF-8 spectrophotometer. The luminescence spectra of $Cs_2NaLuCl_6$, doped with 10 mol.% ^{241}Am (half-life, 432 years), were studied on a DFS-24 spectrometer either without excitation (self-luminescence spectra) or under excitation with an LGI-21 nitrogen pulse laser (λ=337.1 nm). For cooling the crystal to 15 K, we used an MSMR-110N-3.2/20 microcryogenic system with an optical cryostat designed by us and described in Ref. [7].

3. Results and discussion

3.1. Absorption spectra

In Table 1 the sublevel energies of $AmCl_6^{3-}$, which were estimated by the vibronic structure analysis in Ref. [7], are compiled. Also presented are the vibrational (phonon) frequencies associated with the corresponding zero-phonon transitions. Separated by oblique stroke are the frequencies of the longitudinal (LO) and lower-energy transverse (TO) optical phonons in the corresponding doublets (which can appear in the elpasolite spectra for the F_{1u} vibrational modes: ν_3, ν_4, ν_8 and ν_9). In detail, the vibronic spectra of

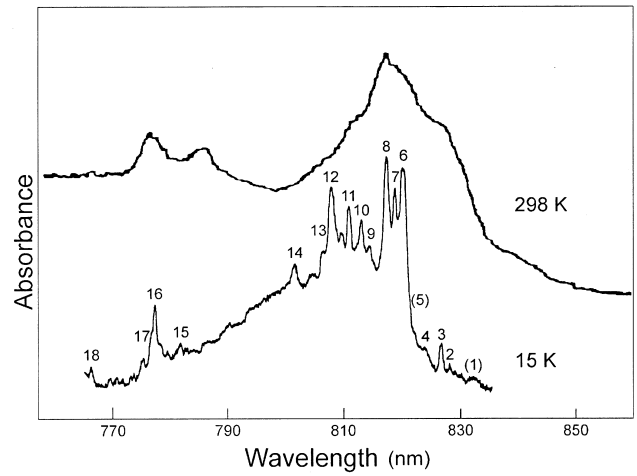

Fig. 1. Absorption spectra of $Cs_2NaLuCl_6:Am^{3+}$ in the region of the $^7F_6 \leftarrow {}^7F_0$ transition. From here on, the values in parentheses in figures and tables refer to positions of the electronic sublevels estimated from the vibronic spectra.

$Cs_2NaLuCl_6:Am^{3+}$ in the regions of the ($^5G_2$, $^5D_2$, $^5L_6$, $^7F_4$, $^7F_2$)$\leftarrow {}^7F_0$ transitions are presented in Ref. [7], along with the assignments for all the sets of vibronic frequencies.

In Fig. 1, the 0–0 transition at 12 788 cm^{-1} (denoted as IV in Table 2) can be rather distinctly localized as the origin line for the ν_6-, ν_4- and ν_3-assisted cold vibronic transitions. Both cold and hot ν_6-assisted vibronic transitions associated with the sublevel IV can be seen in the region 770–790 nm at room temperature. A tentative localization of sublevels III and II at 12 210 and 12 160 cm^{-1} from the spectrum at 15 K in Fig. 1 can be supported by the analysis of the difference spectra in Fig. 2. In these kinds of spectra, the hot vibronic lines should manifest themselves as broad dips, possibly with a complex struc-

Table 1
Sublevel energies of Am^{3+} in the $Cs_2NaLuCl_6$ crystal from the absorption spectra

J level	Sublevel energy (cm^{-1})			Vibrational frequencies (cm^{-1}) at 77 K				
	298 K	77 K	15 K	ν_3	ν_4	ν_6	ν_8	ν_9
$^7F_2$	5003	4992	4989	239	93[a]	72[a]		53/41[a]
$^7F_2$	5410	5408	5411	254/242		73[a]	185	42[a]
$^7F_4$	9071	9050	9048	241		72[a]		
$^7F_4$	9630	9619	9617			73[a]	153[b]	
$^7F_4$	9653	9652	9655	239	94[a]		164[b]	
$^5L_6$	18 984	18 950	18 945	262/236		74[a]	164	37/23
$^5L_6$	19 384	19 365	19 356	247	113[b]	78[a]	167	33[a]
$^5L_6$		19 488	19 485	242	114[b]	74[a]	162	
$^5L_6$	19 507	19 503	19 508	241		75[a]	180	
$^5D_2$, $^5G_2$	20 852	20 809	20 790	253/236		72[a]		41[a]
	21 233	21 206	21 243		94			
$^5D_2$, $^5G_2$	21 550	21 530	21 524			73[a]	167	42[a]
$^5D_2$, $^5G_2$	21 815	21 820	2 1808	253/236	91[a]	71[a]		45[a]

[a]Average for the frequencies associated with the cold and hot vibronic lines.
[b]Frequencies for the hot vibronic lines. Frequencies for the cold vibronic lines are not marked.

Table 2
Zero-phonon and vibronic transitions energies from the absorption spectrum of $Cs_2NaLuCl_6:Am^{3+}$ ($^7F_6 \leftarrow {}^7F_0$ region) at 15 K

Energy, E (cm^{-1})	Peak no. in Fig. 1	Assignment
(12 025)	(1)	I (0–0)
12 075	2	I+50 (ν_9)
12 097	3	I+72 (ν_6)
12 134	4	I+109 (ν_4)
(12 160)	(5)	II (0–0)
12 190	6	I+165 (ν_8)
12 210	7	III (0–0)
12 232	8	II+72 (ν_6)
12 276	9	I+251 (ν_3)
12 296	10	III+86 (ν_4)
12 330	11	II+170 (ν_8)
12 376	12	III+166 (ν_8)
12 403	13	II+243 (ν_3)
12 430		not assigned
12 475	14	III+265 (ν_3)
(12 788)	15	IV (0–0)
12 862	16	IV+74 (ν_6)
12 895	17	IV+107 (ν_4)
13 045	18	IV+257 (ν_3)

ture. It is impossible to precisely identify the frequencies for the hot transitions from the difference spectra in Fig. 2. Nevertheless, one can approximately specify the ranges of occurrence of the dips as 822 and 828 nm. The fact that these dips closely correspond to the hot vibronic frequencies associated with the electronic sublevels at 12 210 and 12 160 cm^{-1} is an indirect evidence in favor of the localization of sublevels III and II from the spectrum at 15 K.

One more electronic sublevel (I in Table 2) can be localized as the origin line for the ν_9-, ν_6- and ν_4-assisted cold vibronic transitions (nos. 2–4 in Fig. 1). The two remaining sublevels (of six for $J=6$ in O_h symmetry), which are the highest in energy and should be close to IV at 12 788 cm^{-1} (as follows from the calculated data in Table 4), cannot be revealed in the spectra in Fig. 1. Several very weak lines in this region are possibly associated with the transitions to the unidentified sublevels of the $^7F_6$ level.

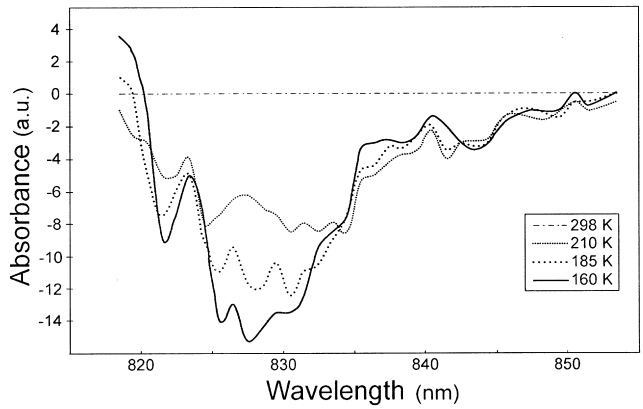

Fig. 2. Difference spectra of $Cs_2NaLuCl_6:Am^{3+}$ in the long-wave part of the $^7F_6 \leftarrow {}^7F_0$ transition. The curves for 210, 185, and 160 K were obtained by subtracting the corresponding absorption spectra of the cooled sample from the room temperature spectrum.

3.2. Luminescence spectra

Fig. 3 shows not only decreases in the intensities of the hot vibronic transitions on lowering the temperature (see assignments in Table 3), but also the long-wave shift of the whole band manifold, which is evidently due to the decrease in the population of the higher electronic sublevels in the $^5L_6$ level. Analysis of the temperature dependence of the line intensities in Fig. 3 makes it possible to assign the five (of six in O_h symmetry for $J=6$) electronic sublevels and some of the corresponding vibronic levels (Table 3). The line at 19 169 cm^{-1} manifests itself at temperatures when the sublevels at 19 356 (IV)

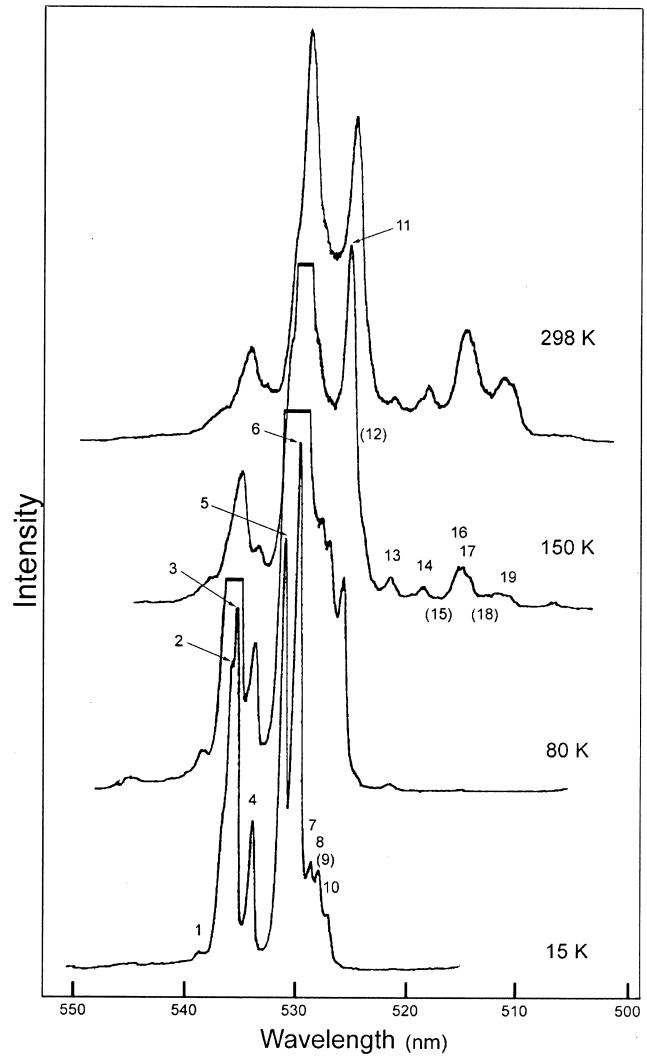

Fig. 3. Self-luminescence spectra of $Cs_2NaLuCl_6:Am^{3+}$ in the region of the $^5L_6 \rightarrow {}^7F_0$ transition.

Table 3
Zero-phonon and vibronic transitions energies from the self-luminescence ($^5L_6 \rightarrow {}^7F_0$) spectra of $Cs_2NaLuCl_6:Am^{3+}$

Energy, E (cm^{-1})		Peak no. in Fig. 3	Assignment
150 K	15 K		
18 590	18 560	1	I−260 (ν_3)
	18 656	2	I−164 (ν_8)
18 686	18 670	3	I−150(ν_8)
18 746	18 724	4	I−97 (ν_4)
	18 820	5	I (0–0)
18 880	18 866	6	II−77 (ν_6)
	18 912	7	II−31 (ν_9)
	18 934	8	Not assigned
(18 957)	(18 943)	(9)	II (0–0)
	18 968	10	Not assigned
19 034		11	II+77 (ν_6)
(19 097)		(12)	III (0–0)
19 169		13	III+72 (ν_6)
19 278		14	IV−78 (ν_6)
(19 356)		(15)	IV (0–0)
19 397		16	V−71 (ν_6)
19 434		17	IV+78 (ν_6)
(19 468)		(18)	V (0–0)
19 540		19	V+72 (ν_6)

and 19 468 cm^{-1} (V) must be frozen out. Also, this line can belong to neither of the two lowest sublevels (I or II). Thus, by assigning the line at 19 169 cm^{-1} to the hot ($+\nu_6$) vibronic component of the intermediate energy sublevel III, we can supposedly localize this sublevel at 19 097 cm^{-1}. With this assignment, the corresponding cold component (19 097−72=19 025 cm^{-1}) is veiled at higher temperatures by the intense line at 19 034 cm^{-1} (no. 11), while at lower temperatures the electronic sublevel III at 19 097 cm^{-1} proves frozen out. Of course, the above assignment of the sublevel III needs additional evidence.

In the luminescence spectra we could not reveal the highest sublevel of the $^5L_6$ level (19 508 cm^{-1} in Table 1). In the low-temperature (12–15 K) absorption spectra, the sublevels at 19 508 and 19 485 cm^{-1} and the corresponding vibronic energy levels are well-separated. In the luminescence spectra, these two sublevels prove frozen out at temperatures when the bands remain fairly broad.

It should be noted that the vibronic pattern associated with the lowest electronic sublevel at 18 820 cm^{-1} (Table 3) does not involve the $\nu_6(\Gamma_5)$-assisted transition which is typically the most intense in the chloroelpasolite vibronic patterns. This suggests the Γ_1 symmetry for the sublevel revealed. Indeed, in terms of the Judd–Ofelt intensity theory the transition probability is determined by the squared matrix element $\langle\Psi_1|\partial H/\partial Q\cdot E|\Psi_2\rangle$ where Ψ_1 and Ψ_2 are the wavefunctions for the initial and final states, respectively; Q is the vibrational coordinate; E is the vector of the intensity of the electric component of the light wave (Γ_4 symmetry); and H is the Hamiltonian for the electronic–vibrational interaction (Γ_1 symmetry). In the case that the initial and final states belong to Γ_1 symmetry, the matrix element is non-zero only for vibrations of the Γ_4 symmetry.

In the luminescence spectra excited by a nitrogen pulse laser, we observe a number of additional lines associated possibly with the transitions from higher excited levels. These lines remain to be assigned, as well as some very weak lines in the self-luminescence spectra in Fig. 3.

3.3. Crystal field calculation for the $AmCl_6^{3-}$ complex

The principles of the calculational procedure within both the relativistic and nonrelativistic approximations were presented in Refs. [11–13]. Thus, we restrict ourselves to some comments on this subject. The secular equation was composed with a basis set of the atomic wavefunctions for Am^{3+} in the $LaCl_3$ crystal, which were kindly provided by Dr. William T. Carnall (Argonne National Laboratory, USA). The level energies and the atomic (free ion) parameters corresponding to these wavefunctions are presented in Ref. [14]. To adjust the baricenters of the calculated levels to those observed in the experiment, additional factors were introduced for each J level, i.e. $p(2^{S+1}LJ)$. These factors are given in Table 4. The root-mean-square (r.m.s.) deviations, Δ, were calculated for the split levels only, as the positions of the nonsplit levels always coincide with those of the observed ones, owing to the factors introduced.

Experimental values for the sublevel energies in Table 4 were taken from Tables 1–3 and those for the $^7F_1$ and $^5D_1$ level energies, from Refs. [8,9,11].

The sublevel assignments to J levels and to Γ_i irreducible representations in Table 4 were chosen in such a way that the r.m.s. deviation of the calculated energies from the experimental values is at minimum. The change from the nonrelativistic to relativistic version of calculation affords a noticeably better agreement between the experimental and calculated sublevel energies (Δ decreases from 42.0 to 36.5 cm^{-1}). At the same time, it should be mentioned that both CF parameters and r.m.s. deviations are most strongly dependent on the assignments for the region of transitions to the $^5G_2$ and $^5D_2$ levels (20 000–22 000 cm^{-1} in Tables 1 and 4). With assignments taken in Table 4, the relationship between the relativistic CF (RCF) parameters, i.e. $B_0^4(5/2)>B_0^4(7/2)$, proves opposite to that expected in view of a greater extension of the $f_{7/2}$ function. An alternative assignment of the sublevels in the region discussed (i.e. $^5G_2$, 20 809 and 21 530 cm^{-1}; $^5D_2$, 21 820 cm^{-1}) affords, at the cost of a certain rise in the r.m.s. deviations (Δ=51.8 and 42.8 cm^{-1} for nonrelativistic and relativistic versions, correspondingly) a 'regular' relationship between the RCF parameters. It is important that in the same region (20 000–22 000 cm^{-1}) we revealed a sublevel at 21 206 cm^{-1} (Table 1), which remains to be assigned. If our assumption that this sublevel belongs to the $^5H_3$ level is correct, the account of this level in the calculational procedure can noticeably affect the CF

Table 4
Energy levels of the $AmCl_6^{3-}$ complex

Experimental value (cm^{-1})	Calculated values (cm^{-1}) and assignments				J level
	Non-relativistic		Relativistic		
0	0.0	Γ_1	0.0	Γ_1	$^7F_0$
2725	2725.1	Γ_4	2725.1	Γ_4	$^7F_1$
4992	4971.4	Γ_3	4990.6	Γ_3	$^7F_2$
5408	5429.6	Γ_5	5409.4	Γ_5	
—	7301.6	Γ_2	7214.8	Γ_2	$^7F_3$
—	7484.4	Γ_5	7489.5	Γ_4	
—	7538.6	Γ_4	7520.5	Γ_5	
9050	9107.2	Γ_5	9069.9	Γ_5	$^7F_4$
—	9461.2	Γ_3	9457.5	Γ_3	
9619	9588.1	Γ_4	9605.4	Γ_4	
9652	9624.5	Γ_1	9644.5	Γ_1	
—	10 858.6	Γ_4	10 751.9	Γ_5	$^7F_5$
—	10 884.8	Γ_3	10 840.5	Γ_4	
—	10 959.1	Γ_5	10 888.4	Γ_3	
—	11 205.0	Γ_4	11 394.9	Γ_4	
12 025	12076.1	Γ_3	12 088.9	Γ_3	$^7F_6$
12 160	12 120.9	Γ_5	12 122.2	Γ_5	
12 210	12 209.6	Γ_2	12 185.1	Γ_2	
—	12 246.1	Γ_1	12 215.2	Γ_1	$^5D_0$
12 788	12 793.0	Γ_5	12 805.8	Γ_5	$^7F_6$
—	12 842.7	Γ_4	12 849.3	Γ_4	
—	12 905.2	Γ_1	12 927.0	Γ_1	
16 850	16 850.0	Γ_4	16 850.0	Γ_4	$^5D_1$
18 820	18 875.4	Γ_1	18 879.9	Γ_1	$^5L_6$
18 950	18 957.7	Γ_4	18 958.6	Γ_4	
19 097	19 053.4	Γ_5	19 067.2	Γ_5	
19 365	19 350.4	Γ_2	19 343.6	Γ_2	
19 488	19 478.1	Γ_5	19 476.3	Γ_5	
19 503	19 508.2	Γ_3	19 497.4	Γ_3	
—	20 768.6	Γ_3	20 801.7	Γ_3	$^5D_2$
20 809	20 808.9	Γ_5	20 808.9	Γ_5	
21 530	21 454.3	Γ_3	21 469.1	Γ_3	$^5G_2$
21 820	21 903.6	Γ_5	21 886.8	Γ_5	
—	22 140.3	Γ_4	22 124.9	Γ_4	$^5H_3$ ($^5G_3$)
—	22 230.2	Γ_2	22 223.7	Γ_5	
—	22 234.0	Γ_5	22 263.3	Γ_2	

CF: B_0^4=4428±168 cm^{-1}, B_0^6=2±107 cm^{-1}, Δ=42.0 cm^{-1}, $p(^7F_1)$=0.9932, $p(^7F_2)$=0.9903, $p(^7F_4)$=0.9856, $p(^7F_6)$=1.0011, $p(^5D_1)$=0.9737, $p(^5L_6)$=0.9810, $p(^5D_2)$=0.9608, $p(^5G_2)$=0.9907. RCF: $B_0^4(5/2)$=5184±360 cm^{-1}, $B_0^4(7/2)$=3939±310 cm^{-1}, $B_0^4(5/2, 7/2)$=4726±230 cm^{-1}, $B_0^6(7/2)$=−1277±330 cm^{-1}, $B_0^6(5/2, 7/2)$=561±108 cm^{-1}, Δ=36.5 cm^{-1}, $p(^7F_1)$=0.9926, $p(^7F_2)$=0.9891, $p(^7F_4)$=0.9873, $p(^7F_6)$=0.9990, $p(^5D_1)$=0.9739, $p(^5L_6)$=0.9812, $p(^5D_2)$=0.9610, $p(^5G_2)$=0.9904.

parameters, especially those within the relativistic approximation.

4. Conclusion

Further experiments are needed to confirm some of the presented CF assignments and to localize the lacking sublevels, in particular, for the higher-energy excited states in the $5f^6$ configuration. Also, modification of the calculational procedure so as to minimize the r.m.s. deviations will be the aim of future research. The results in recent works by other authors [15,16] encourage further optical spectroscopic studies on the electronic structure of the trivalent actinide ions situated at the sites of the O_h symmetry.

Acknowledgements

The authors are extremely thankful to Dr. Solange Hubert (Orsay, France) who provided them with the luminescence spectra of $Cs_2NaYCl_6:Am^{3+}$ prior to publication; a comparison analysis of these and our spectra was of great value for our assignments. We are also grateful to Drs. Solange Hubert and Eric Simoni for presenting us with the results of their CF calculations based on our data given in Ref. [17]. This research was sponsored by Russian

Foundation for Basic Research under Grant No. 97-03-33400.

References

[1] P. Tanner, V.V. Ravi Kanth Kumar, C.K. Jayansankar, M.F. Reid, J. Alloys Compounds 215 (1994) 349–370.
[2] Yu.A. Barbanel', V.P. Kotlin, G.P. Chudnovskaya, Radiokhimiya 16 (1974) 889.
[3] K.W. Bagnall, J.B. Laidler, M.A.A. Stewart, J. Chem. Soc. (A) (1968) 133-136.
[4] L.R. Morss, M. Siegal, L. Stenger, N. Edelstein, Inorg. Chem. 9 (1970) 1771–1775.
[5] Yu.A. Barbanel', R.B. Dushin, V.V. Kolin, V.P. Kotlin, G.P. Chudnovskaya, in: Proc. 2nd Int. Conf. Electr. Str. Actin., Wroclaw, Poland, 1976, pp. 179–183.
[6] Yu.A. Barbanel', R.B. Dushin, N.K. Mikhailova, G.P. Chudnovskaya, Radiokhimiya 21 (1979) 706–713.
[7] Yu.A. Barbanel', R.B. Dushin, V.V. Kolin, V.P. Kotlin, S.N. Nekhoroshkov, M.V. Pen'kin, G.P. Chudnovskaya, Radiokhimiya 39 (1997) 46–53.
[8] G.P. Chudnovskaya, Yu.I. Gavrish, Yu.A. Barbanel', Radiokhimiya 30 (1988) 46–52.
[9] Yu.A. Barbanel', G.P. Chudnovskaya, Yu.I. Gavrish, R.B. Dushin, V.V. Kolin, V.P. Kotlin, J. Radioanalyt. Nucl. Chem. 143 (1990) 113–129.
[10] Yu.A. Barbanel', V.V. Kolin, V.P. Kotlin, Radiokhimiya 33 (1991) 29–32.
[11] A.L. Ankudinov, Yu.A. Barbanel', R.B. Dushin, G.P. Chudnovskaya, Radiokhimiya 34 (1992) 47–55.
[12] R.B. Dushin, L.D. Shcherba, Radiokhimiya 34 (1992) 107–118.
[13] R.B. Dushin, S.N. Nekhoroshkov, Radiokhimiya 38 (1996) 210.
[14] W.T. Carnall, An^{3+} Free Ion Eigenvector Tables, Report ANL 89/39, Argonne National Laboratory, Argonne, IL, 1989.
[15] S. Hubert, P. Thouvenot, N. Edelstein, Phys. Rev. B 48 (1993) 5751–5760.
[16] N.M. Edelstein, J. Alloys Compounds 223 (1995) 197–203.
[17] Yu.A. Barbanel', R.B. Dushin, G.P. Chudnovskaya, V.V. Kolin, V.P. Kotlin, S.N. Nekhoroshkov, M.V. Pen'kin, in: 4th Int. Conf. Nucl. Radiochem. NRC4, Extended Abstracts, Orsay, France, 1996, C-P15; Radiochim. Acta 78 (1997) 69–72.